This version of the article has been accepted for publication in *Springer – Annals of Telecommunications* on October 28, 2022, after peer review but is not the version of the Article published by the journal and does not reflect post-acceptance improvements, or any corrections. The published Article is available online at: http://dx.doi.org/10.1007/s12243-022-00932-9. Use of this Accepted Version is subject to the publisher's Accepted Manuscript terms of use.

Evaluation and projection of 4G and 5G RAN energy footprints: The case of Belgium for 2020–2025

Louis Golard[1*], Jérôme Louveaux[1] and David Bol[1]

[1]ICTEAM Institute, UCLouvain, Louvain-la-Neuve, Belgium.

*Corresponding author(s). E-mail(s): louis.golard@uclouvain.be;
Contributing authors: jerome.louveaux@uclouvain.be; david.bol@uclouvain.be;

Abstract

Energy consumption of mobile cellular communications is mainly due to base stations (BSs) that constitute radio access networks (RANs). 5G technologies are expected to improve the RAN energy efficiency while supporting the forecasted growth in data traffic. However, the evolution of the absolute RAN energy consumption with 5G deployment is not clear. Moreover, existing BS power models are mostly derived from legacy equipment. Therefore, this work presents a method to evaluate and to project the total energy consumption of broadband RANs. We use on-site up-to-date measurements to determine power models of 4G BSs, showing a linear relationship between power consumption and data traffic with a static traffic-independent power component. We then build a prospective power model of 5G BSs by scaling 4G models with respect to bandwidth, number of data streams, and expected technological improvements. We apply this method to the RANs in Belgium over the 2020-2025 period for six scenarios of 5G deployment. Results show that the static energy consumption accounts for a major part of the total RAN energy consumption, which implies that concurrently operating 4G and 5G RANs consumes more energy than using only one generation. The sleep mode feature of 5G technology can reduce its RAN static energy consumption, improving energy efficiency by 10 times compared to 4G. Finally, we estimate the absolute carbon footprint of 4G and 5G RANs by considering embodied and operating greenhouse gas emissions. They follow a clear upward trend for scenarios with extensive 5G deployment.

Keywords: Base station power model, 5G deployment, Radio access network, Energy footprint, Rebound effect

1 Introduction

Nowadays, information and communication technologies (ICTs) are responsible for an annual electricity consumption of around 1400 TWh, and an annual carbon footprint of about 1.4 $GtCO_2e$, which represents 6-7% and 2-4% of the global electricity and carbon footprints, respectively [1–9]. Among ICTs, mobile cellular communications benefited over the last decade from strong reductions in energy and carbon intensity of data transfer. However, their absolute energy and carbon footprints have instead grown, due to the exponential growth in data traffic [1, 2, 4, 10, 11]. This trend could continue in the future given the expected rise in mobile broadband Internet access by human subscribers, the advent of machine-to-machine (M2M) communications, and the development of new connected applications [12–14]. Most of the mobile data traffic is currently supported by 4G networks, but the increase in throughput and the new constraints of real-time communications could saturate existing networks and may require a more advanced technology such as 5G [15]. The infrastructure supporting mobile communications can be divided into four segments: (i) the end-user devices, (ii) the radio access network (RAN), (iii) the core network, and (iv) the data centers. Previous studies estimated that the RAN typically accounts for two third of the electricity consumption and one third of the carbon footprint of this sector [1, 4, 10, 16], which justifies to focus first on this segment.

Research in this field is primarily seeking to improve the energy efficiency, with limited attention to the absolute energy consumption [17]. In contrast, the main objective of this work is to present a method to evaluate and to project the absolute energy consumption of broadband RANs. Structures of these RANs are modeled using a bottom-up approach as described in an existing framework from the EARTH project [18, 19]. Yet, in order to avoid the need for modeling the communication channel and the signal propagation between base stations (BSs) and mobile users, we introduce models which directly link the average BS power consumption with the average data traffic. In the literature, existing BS power models derived from actual measurements are mostly based on legacy equipment [20–23]. In order to reflect current 4G LTE BSs, we fit parameters of their power models to on-site up-to-date measurements provided by an operator. We then build a prospective power model of 5G NR BSs by scaling 4G models with respect to bandwidth, number of data streams, and expected technological improvements. We also estimate the absolute carbon footprint of 4G and 5G RANs by considering embodied and operating greenhouse gas (GHG) emissions. In this work, the whole method is applied to broadband RANs in Belgium for six scenarios of 5G deployment from 2020 to 2025.

This paper is organized in four sections. Section 2 explains the methodology used to model country-wide RANs. Then, Section 3 investigates the practical structure of 4G and 5G RANs in Belgium, defines power models of 4G and 5G BSs, and determines the daily traffic profile. Next, Section 4 presents different scenarios of 5G deployment in Belgium, and the corresponding mobile data traffic evolution by 2025. Finally, total RAN energy and carbon footprints are evaluated in Section 5.

2 Methodology

Country-wide RANs are modeled using a bottom-up approach, allowing to study current 4G RANs as well as different future 5G RANs. This section first introduces an existing framework that assesses the RAN power consumption and then explains how it is adapted in this work.

2.1 Existing framework

The EARTH project defined the energy efficiency evaluation framework (E^3F) [18, 19] which divides the non-uniform *large-scale* deployment of RANs into several homogeneous *small-scale* systems. In addition, the *long-term* traffic profile is split into successive *short-term* periods of constant traffic.

Evaluations are conducted for the set of short-term traffic loads in each small-scale deployment areas to provide performance metrics such as the throughput, the power consumption, and the energy efficiency. For each small-scale short-term configuration, the instantaneous traffic is modeled statistically, reflecting the packet transfer of different types of devices and applications, e.g., file downloading or video streaming. The users are assumed to be uniformly distributed in regular hexagonal cells. The transmitted (TX) power of BSs are then computed, and a power model is applied to estimate their power consumption. Hence, it requires estimating the TX power for multiple channel conditions between the BSs and the mobile users. These computations can be carried out by a system-level simulation platform.

The large-scale model captures the RAN deployment over a whole country based on the population density. The long-term traffic profile models the data traffic demand over time, for instance over one day. The key assumption is that the traffic load in an area is directly related to its population density. The E^3F considers six small-scale deployment areas: super dense urban (SDU), dense urban (DU), urban, suburban and rural areas, as well as wilderness. SDU reflects city centers with extreme traffic peaks, while wilderness corresponds to sparsely populated areas. The weighted sum of small-scale short-term metrics over the mix of deployment areas and over the traffic profile loads yields the overall large-scale long-term metrics.

The version of the Article published by the journal is available at: http://dx.doi.org/10.1007/s12243-022-00932-9.

2.2 Proposed method

The use of E^{3}F requires modeling signal propagation from BSs to mobile users in all small-scale short-term systems, and to run numerous simulations to achieve a statistically representative sample. Such simulations are sensitive to the implementation of different BS features that are not known in practice, such as the power allocation strategies and the scheduling algorithms [24]. In addition, the evaluation of the RAN power consumption over one day does not require modeling the instantaneous data transfer but only studying average traffic patterns over meaningful time intervals. In this work, we use empirical power models for small-scale short-term evaluations over time intervals of one hour. These models directly link the average power consumption of BSs to their average throughput, respectively $P_{BS,ij}(t)$ (in W) and $R_{ij}(t)$ (in Mbps). The subscript i stands for the deployment area and j represents the BS type. The behavior of power models is not known a priori, but we assume that they can be derived from on-site measurements.

The rest of the methodology is similar to the E^{3}F. The country territory is divided into N_{areas} deployment areas of specific population densities, and we consider N_{types} types of BSs with different features and power models. In the country-wide RAN, each small-scale system configuration (i, j) appears N_{ij} times. The traffic profile follows an hour-by-hour pattern and $R_{ij}(t)$ depends on the population size covered by the cell. From short-term to long-term, the BS power consumption is integrated throughout 24 hours to obtain the daily BS energy consumption E_{ij} (in kWh). From small-scale to large-scale, BS energy consumptions are summed according to coefficients N_{ij}. Considering N_{op} operators with identical RAN deployments, the daily energy consumption of all RANs is

$$E_{tot} = N_{op} \sum_{i=1}^{N_{areas}} \sum_{j=1}^{N_{types}} N_{ij} E_{ij}, \qquad (1)$$

where the energy consumption of one BS in configuration (i, j) is

$$E_{ij} = \int_0^{24} P_{BS,ij}\left(R_{ij}(t)\right) \,\mathrm{d}t. \qquad (2)$$

The annual energy consumption is $365 \times E_{tot}$ because we assume that the daily traffic profile remains unchanged throughout the year.

3 System model

The bottom-up model of 4G RANs in Belgium is built by analyzing the RAN deployment of one Belgian operator. Empirical power models of 4G BSs are then established using on-site measurements. Next, a prospective power model of 5G BSs is proposed based on technical and practical assumptions. Finally, on-site measurements are also used to derive a typical mobile traffic profile.

3.1 Structure of 4G RANs

In Belgium, there are three mobile network operators (MNOs) that operate their own 4G RAN: Proximus, Orange and Base/Telenet, yielding $N_{op} = 3$. According to the Belgian Institute for Postal Services and Telecommunications (BIPT), a very large part of the territory is satisfactorily covered by 4G for the three MNOs, except for the large unpopulated forests [25]. In this work, we assume full 4G coverage for the three MNOs. From the open databases of transmitting antennas in Belgium [26–28], the distribution of 4G sites is similar for all MNOs. Indeed, MNOs primarily provide coverage over the whole territory [18], even if they do not have the same market share [29]. Therefore, we assume that the deployment strategies of all operators are identical with the same number of BSs in each deployment area. Consequently, we analyze only one of the three 4G RANs to determine coefficients N_{ij}^{4G} using positioning coordinates of its 4G LTE macro sites.

Cells of the 4G cellular network are determined by Voronoi tessellation with 4G sites as centroids. The population covered by each site is estimated by computing the number of inhabitants in its respective cell, based on demographic data reported for a grid of squares of 1 km^2 over the whole territory [30]. The population density of each cell is calculated by dividing its estimated population by the area of its Voronoi region. Each 4G site is then classified according to the population density of its cell. The same deployment areas as E^{3}F are considered such that $N_{areas} = 6$. Figure 1 depicts the Voronoi tessellation of Belgium's territory and the classification of 4G cells.

The version of the Article published by the journal is available at: http://dx.doi.org/10.1007/s12243-022-00932-9.

Table 1 Cell characteristics of the six deployment areas (std. = standard deviation)

	Population density [citizens/km^2]		Area [km^2]		Population [citizens]		
Deployment areas	Class interval	Mean	Mean	Std.	Mean	Std.	Share
Wilderness	< 50	29	26.30	17.01	759	636	5.9%
Rural	[50; 250[	134	15.45	8.89	2073	1103	23.7%
Suburban	[250; 750[	420	7.35	3.95	3088	1611	30.0%
Urban	[750; 1500[	1015	3.69	2.17	3749	2044	13.1%
Dense urban	[1500; 10000[	2925	1.37	0.99	4004	1775	22.2%
Super dense urban	≥ 10000	14828	0.33	0.12	4855	1698	5.1%

Classification intervals and corresponding cell distribution are given in Table 1 with cell area and cell population statistics for each class.

In the studied RAN, 92% of 4G BSs have 3 sectors, and hence we model all BSs with 3 sectors. 4G BSs also use either one frequency band (27%), two bands (51%), three bands (21%) or four bands (1%). This last case is ignored in the model. All frequency bands use a frequency division duplex (FDD) paired spectrum, meaning that for each carrier, one part of the spectrum is allocated to downlink (DL) and another part of the same bandwidth, to uplink (UL) [31]. The first 4G frequency band deployed at a site is the 800 MHz coverage band with 2×10 MHz, the second is the 1800 MHz band with 2×20 MHz, and the third is the 2600 MHz band with 2×20 MHz. The more densely populated the deployment area, the greater the share of 3-band BSs, offering more overall bandwidth for devices capable of carrier aggregation. No 1-band BS is deployed in SDU. Two main multiple-input multiple-output (MIMO) antenna configurations are also used: 2T2R antennas comprising two cross-polarized channels and 4T4R antennas consisting of two large beams with two cross-polarized channels each, making 4 streams overall. Despite different number of transmitting antennas, the total maximum TX power per MHz does not change between these two configurations, i.e., 4W/MHz. 98% of the 3-band BSs use 4T4R while other BSs mainly use 2T2R. In the model, we consider only three main types of 4G BSs, respectively the 1-band, 2-band and 3-band 4G BSs, resulting in $N_{types}^{4G} = 3$. Their main features are summarized in Table 2.

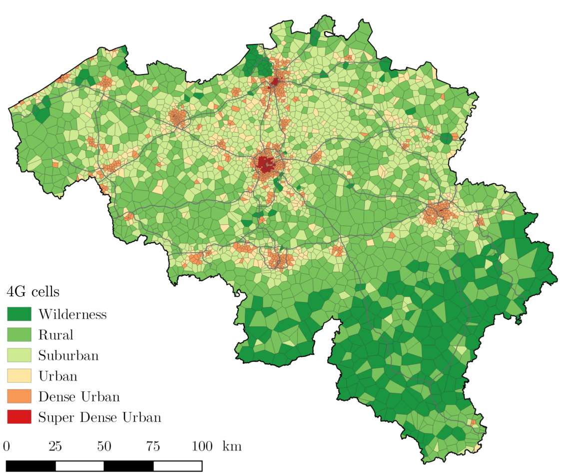

Fig. 1 Voronoi tessellation of Belgium's territory with 4G sites as centroids and classification of cells into six deployment areas based on their population density

3.2 Empirical power model of 4G BSs

The large-scale model of the 4G RAN is composed of $N_{areas} \times N_{types}^{4G} = 18$ small-scale system configurations, for which 4G BS power models are empirically derived from on-site measurements of data traffic and power consumption. These operator-provided measurements come directly from on-site monitoring systems that differentiate the 4G part of the site from other installed mobile generations (e.g., 2G and 3G). The measured data traffic is the sum of DL and UL data volumes on all 4G bands. The measured power consumption includes the digital baseband unit, the radio frequency transceivers and the power amplifiers of all sectors but excludes the active cooling system, the main supply and the power converters that are usually shared by all mobile generations. For this work,

The version of the Article published by the journal is available at: http://dx.doi.org/10.1007/s12243-022-00932-9.

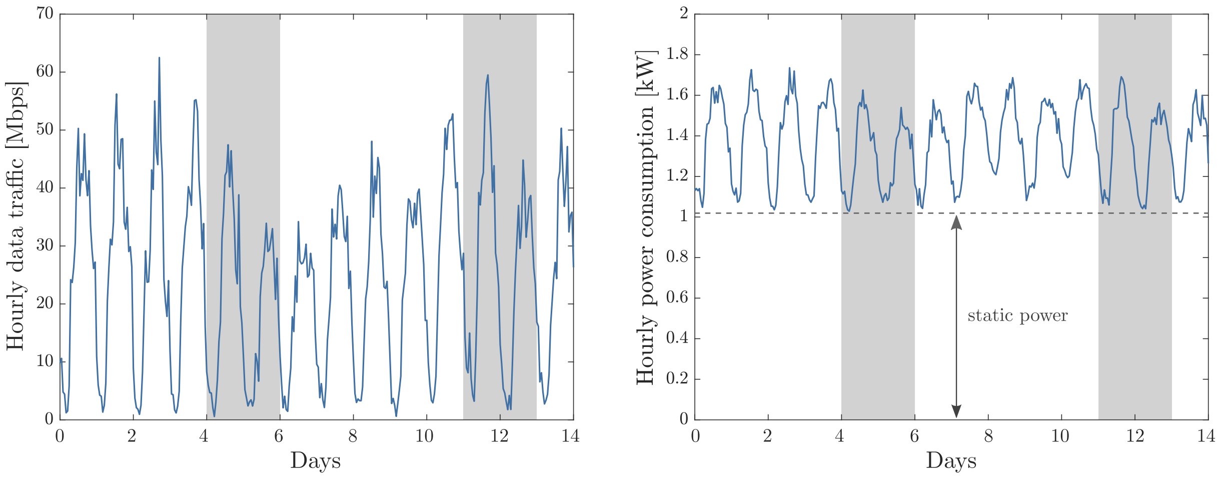

(a) (b)

Fig. 2 Example of hourly measurements of (a) mobile data traffic and (b) power consumption of one base station during 14 days with shaded areas highlighting weekend days

we randomly sampled 5 BSs per small-scale configuration from all 4G BSs in the studied RAN to include different manufacturers and production years. An example of hourly measurements performed during 14 days in 2021 is shown in Fig. 2. A periodic pattern is clearly visible for the data traffic and the power consumption following the day and night alternation. The minimum data traffic is close to zero, but the power consumption oscillates above a non-zero level, which indicates a static power component.

Linear regressions are computed between the two measured parameters for each BS individually,

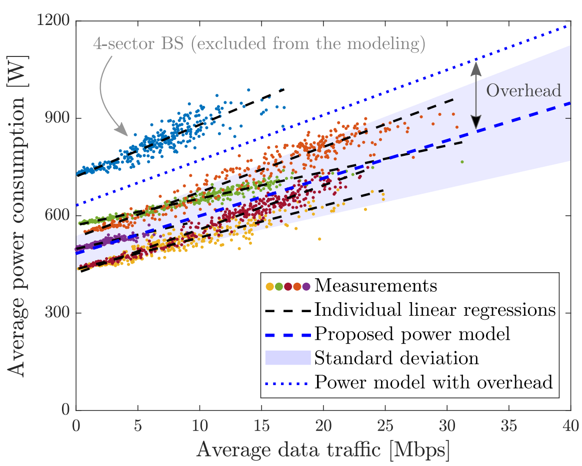

Fig. 3 Linear regressions of individual base stations in one small-scale system configuration compared to the proposed linear model, its standard deviation, and the complete power model including the supply and cooling overheads

using a robust bisquare method. The goodness-of-fit is determined with the R-squared (R^2) which is 0.90 on average, ranging from 0.85 to 0.95. It means that there is a strong linear relationship between power consumption and data traffic over the measurement range, allowing to rely on linear models. Examples of such regressions are shown in Fig. 3. They all consist of a constant and a variable component that reflect the *static* (traffic-independent) and the *dynamic* (traffic-dependent) power consumption, respectively. This shape is consistent with other studies in the literature [16, 18–23]. No discontinuity is observed during the low-traffic hours, which suggests that there is no *sleep mode* implemented in these BSs.

Despite the random sampling of sites, BSs with the same number of bands in the same deployment area behave similarly, which supports the analysis per small-scale configuration. Therefore, one power model per configuration is carried out from linear regressions of individual BSs. Actually, the static power is similar for BSs of the same type, regardless of the deployment area. This is meaningful because this power level is only related to the BS architecture, and not to the size of the cell or the signal propagation characteristics, as there is no data transfer. The static power is also higher when there are more bands on the BS, and hence this parameter is estimated for each BS type by averaging intercepts of corresponding individual regressions. In contrast, slopes of linear regressions vary from one deployment area to another.

They are roughly similar for the same type of BS in deployment areas from wilderness to urban but are less steep in DU and even less in SDU. We hypothesize that the significantly smaller cells in these areas requires less TX power to transmit the same amount of data. Slopes of linear power models are estimated by averaging the slopes of individual regressions in corresponding configurations. The values of model parameters are given in Table 4. There is nevertheless a variability across individual regressions related to the same configuration: the standard deviation of their intercepts and slopes are respectively 15% and 25% on average. On top of that, we model the power overhead due to the active cooling system, the main supply and the power converters by using three efficiency coefficients, namely η_{cool}^{4G}, η_{MS}^{4G} and η_{DC}^{4G}, which are each equal to 92% in 4G [32]. The complete 4G BS power model as a function of the throughput is

$$P_{BS,ij}^{4G}\left(R_{ij}^{4G}\right) = \frac{P_{0,j}^{4G} + \Delta_{P,ij}^{4G} \cdot R_{ij}^{4G}}{\eta_{MS}^{4G} \cdot \eta_{DC}^{4G} \cdot \eta_{cool}^{4G}}, \tag{3}$$

where $P_{0,j}^{4G}$ is the no-traffic power consumption (in W) of a 4G BS of type j, and $\Delta_{P,ij}^{4G}$ is the variation of the BS power consumption with traffic (in W/Mbps) in configuration (i, j).

The cell average capacity of each BS type is estimated using the cell average DL and UL spectral efficiencies (SEs) of each frequency band f, expressed by $\gamma_{avg,f}^{DL,4G}$ and $\gamma_{avg,f}^{UL,4G}$ respectively. For a 4G BS of type j, it is given (in Mbps) by

$$C_{avg,j}^{4G} = N_{sect} \sum_{f=1}^{N_{bands,j}} B_f^{4G} \cdot \left(\gamma_{avg,f}^{DL,4G} + \gamma_{avg,f}^{UL,4G}\right), \tag{4}$$

where N_{sect} and $N_{bands,j}$ are respectively the number of sectors and the number of bands of the BS, and B_f^{4G} is the bandwidth of frequency f. In 4G, the useful bandwidth is 9 MHz at 800 MHz and 18 MHz at 1800 MHz and 2600 MHz. We estimate the cell average DL SEs from raw data of a measurement campaign of BIPT, giving 2.1 bps/Hz at 800 MHz, 3.6 bps/Hz at 1800 MHz and 3.9 bps/Hz at 2600 MHz. We then estimate the cell average UL SEs using

$$\gamma_{avg,f}^{UL,4G} = \gamma_{avg,f}^{DL,4G} \cdot \left(\frac{1}{\alpha_{DL}} - 1\right), \tag{5}$$

where α_{DL} is the ratio of DL traffic compared to the total traffic, which is 0.9 in 4G according to on-site measurements provided by the operator.

3.3 Structure of 5G RANs

By 2025, 5G will be deployed in Belgium, but detailed characteristics of 5G RANs are not yet known. Therefore, large-scale 5G deployment must be projected under several assumptions. In 5G NR, two frequency ranges (FRs) can be used: FR1 (below 6 GHz) and FR2 (millimeter waves) [33, 34]. BIPT has no plans to allow the use of FR2 soon in Belgium, but it has authorized the use of the 3.5-GHz band. At that frequency, the three MNOs have access to 50 MHz of bandwidth each [29]. Time division duplex (TDD) is more likely to be used at 3.5 GHz, with a division between UL and DL according to predefined frame structures. In general, TDD schemes give about 75% of time to DL and 25% to UL, which is useful with the asymmetric traffic of mobile users [34]. A key challenge in 5G is to provide a good coverage at higher frequencies having larger signal attenuation. This issue can be mitigated by using directive antennas on both transmitters and receivers to provide beamforming gains [15, 34]. In the field, tests show that massive MIMO at 3.5 GHz could provide a DL coverage similar to passive antennas at 2.1 GHz with the same TX power spectrum density [35]. As a result, it could be feasible to deploy 5G at existing 4G sites. However, UL coverage is worse at 3.5 GHz even with massive MIMO, requiring the support of lower 4G bands for UL in poor channel conditions [34, 35]. In this work, we assume that there is no need to increase the density of 5G sites at 3.5 GHz compared to existing 4G sites. We consider 3-sector macro-BS with 32T32R active antennas having the same total maximum TX power per MHz as 4G, which is consistent with existing BSs on the market. Table 2 gives the main features of the studied 5G BS.

3.4 Prospective power model of 5G BSs

Since 5G is not widely deployed in Belgium at the time of this study, it is not possible to model the power consumption of 5G BSs using on-site measurements. Instead, prospective 5G power models are proposed using a flexible modeling approach

The version of the Article published by the journal is available at: http://dx.doi.org/10.1007/s12243-022-00932-9.

Table 2 Main features of all types of 4G and 5G base stations considered in the model

Type	Carrier frequency [GHz]	Duplexing scheme	Bandwidth [MHz]	MIMO configuration	Total max. TX power [W]	Number of sectors
4G 1-band	0.8	FDD	10	2T2R	40	3
4G 2-bands	0.8/1.8	FDD	10/20	2T2R	40/80	3
4G 3-bands	0.8/1.8/2.6	FDD	10/20/20	4T4R	40/80/80	3
5G 1-band	3.5	TDD 3:1	50	32T32R	200	3

for cellular BSs [32]. This method allows estimating the actual power consumption of a BS P_{act} by scaling a reference power P_{ref} based on a set of scaling parameters $x \in X$ having each a reference value x_{ref}, an actual value x_{act}, and a specific scaling exponent q_x, as

$$P_{act} = P_{ref} \prod_{x \in X} \left(\frac{x_{act}}{x_{ref}} \right)^{q_x}. \qquad (6)$$

In this work, the actual power of 5G NR BSs is estimated with reference power coming from 4G LTE BSs. We assume that this method is valid for early 5G BSs because their specifications do not greatly differ from up-to-date 4G BSs. The first scaling parameter is the *overall bandwidth* B which is the sum of the bandwidth of all bands of the BS (e.g., for a 2-band 4G BS, $B = 30$ MHz). This parameter reflects the complexity of the digital baseband unit and is proportional to the power consumption of power amplifiers. The other one is the *overall number of data streams* S which is the product of the maximum number of streams per band by the number of bands of the BS (e.g., for a 3-band BS with 4T4R antennas, $S = 12$ streams). This parameter reflects the overall number of transmitting chains. The scaling method only applies to absolute powers and not to power versus traffic slopes of linear models. If we first consider that 5G BS models remain linear as in 4G, we need to use at least two power references to which apply the scaling. The first selected reference is the no-traffic power P_0, and the second one is the power at typical high traffic-load, corresponding to 30% of the maximum load [16]. Indeed, RANs are dimensioned to serve the peak traffic demand and to avoid saturation [18, 19]. From on-site measurements of 4G BSs, we evaluate the average load of the busiest hour as 28% for 1-band BSs, 9% for 2-band BSs, and 8% for 3-band BSs. Therefore, the linear behavior of 4G power models is only verified for traffic well below the cell average capacity. The typical high-traffic power of a 4G BS in configuration (i, j) is

$$P^{4G}_{0.3,ij} = P^{4G}_{0,j} + \Delta^{4G}_{P,ij} \cdot 0.3 \cdot C^{4G}_{avg,j}. \qquad (7)$$

Scaling exponents are determined using pairs of 4G BSs with different combinations of scaling parameters. Those related to $P_{0.3}$ are obtained using models for wilderness to urban areas. Table 3 gives the resulting scaling exponents in a range between zero (independence) and one (linear dependency). The no-traffic power scales according to the third root of the bandwidth, which means that when the bandwidth doubles, P_0 increases slightly (i.e., $2^{0.34} = 1.27$). On the other hand, the high-traffic power evolves almost linearly with the bandwidth. Overall, power scaling due to the number of streams is not very strong.

Technological improvements between 4G and 5G are difficult to predict accurately, but they can be roughly addressed by extending past trends. Hence, for every 2-year technology step, we assume a power reduction of $\sqrt{2}$ for analog circuits, of 2 for digital circuits, and of 4% for power amplifiers [32]. As the power breakdown is not available from on-site measurements, we use an existing power model of cellular BSs [32] to estimate that the analog and digital components are respectively responsible for 14% and 22% of power consumption at no-traffic load,

Table 3 Scaling exponents of 4G base stations

Power load		q_B	q_S
No traffic	P_0	0.34	0.10
High traffic	$P_{0.3}$	0.96	0.12

Table 4 Model parameters of 4G and 5G base stations (measured parameters reported as: mean ± standard deviation)

	$P_{0,j}$ [W]	$\Delta_{P,ij}$ [W/Mbps]		
Type	All areas	Wilderness → Urban	Dense urban	Super dense urban
4G 1-band	495 ± 54	11.6 ±3.1	6.9 ±2.3	N.A.
4G 2-bands	747 ±138	17.6 ±3.7	13.3 ±2.7	11.7 ±3.5
4G 3-bands	1045 ±128	20.2 ±5.1	13.6 ±3.1	8.3 ±3.5
5G 1-band	730	5.4	3.6	2.9

and of 10% and 18% at high-traffic load. The rest comes from power amplifiers, which dominate the BS power consumption. As a result, 5G BSs deployed from 2020 achieve a relative power consumption improvement of 36% at no-traffic load and of 30% at high-traffic load, compared to 4G BSs deployed from 2014. Overhead improvements are also assumed, such that the three efficiency coefficients evolve from 92% to 95% [36].

The power scaling of Eq. 6 from 4G to 5G with the two scaling parameters becomes

$$P_k^{5G} = T_k^{5G} \cdot P_k^{4G} \cdot \left(\frac{B^{5G}}{B^{4G}}\right)^{q_B} \cdot \left(\frac{S^{5G}}{S^{4G}}\right)^{q_S}. \quad (8)$$

where k denotes the traffic load (i.e., 0 or 0.3), T_k^{5G} is the technology improvement factor at load k, and B^{5G}/B^{4G} and S^{5G}/S^{4G} are the ratios of scaling parameters, having respectively q_B and q_S as scaling exponents. The complete power model of 5G BSs is adapted from Eq. 3, as

$$P_{BS,i}^{5G}\left(R_i^{5G}\right) = \frac{P_0^{5G} + \Delta_{P,i}^{5G} \cdot R_i^{5G}}{\eta_{MS}^{5G} \cdot \eta_{DC}^{5G} \cdot \eta_{cool}^{5G}}, \quad (9)$$

The power variation of 5G BS with traffic is

$$\Delta_{P,i}^{5G} = \xi_i \cdot \frac{P_{0.3}^{5G} - P_0^{5G}}{0.3 \cdot C_{avg}^{5G}}. \quad (10)$$

where we model the slope reduction of the 5G power model in DU and SDU areas with $\xi_i < 1$, as observed for 4G BSs. The rough values of ξ_i in these areas are respectively obtained by averaging $\Delta_{P,DU}^{4G}/\Delta_{P,W\to U}^{4G}$ and $\Delta_{P,SDU}^{4G}/\Delta_{P,W\to U}^{4G}$ over all types of 4G BSs. The cell average capacity of 5G BSs with a 3:1 TDD scheme is

$$C_{avg}^{5G} = N_{sect} \cdot B^{5G} \cdot \left(0.75 \cdot \gamma_{avg}^{DL,5G} + 0.25 \cdot \gamma_{avg}^{UL,5G}\right), \quad (11)$$

where cell average SEs are set to $\gamma_{avg}^{DL,5G} = 12$ bps/Hz and $\gamma_{avg}^{UL,5G} = 6$ bps/Hz in DL and UL respectively [37, 38]. Prospective model parameters of 5G BSs are given in Table 4.

Among numerous existing energy saving techniques for 5G BSs [39], the sleep mode (SM) is a feature that reduces the idle-state power consumption [32, 40]. When there is no traffic, this feature sequentially disables BS components over time, leading to sleep powers of different depths. At higher traffic loads, power savings decrease with a non-linear behavior. In this work, we model these savings by a decaying exponential function with respect to the traffic load. Parameters of this function are tuned to fit estimated savings from two studies [41, 42] with default 5G synchronization signal periodicity of 20 ms [33]. With SM, the 5G BS power consumption given by Eq. 9 becomes

$$P_{BS,i}^{5G,SM}\left(R_i^{5G}\right) = P_{BS,i}^{5G}\left(R_i^{5G}\right) \cdot \left(1 - 0.75 \cdot \exp\left(-10 \cdot \frac{R_i^{5G}}{C_{avg}^{5G}}\right)\right). \quad (12)$$

The non-linear model starts at no traffic with a sleep power 75% smaller than P_0^{5G} and tends to the linear model at high traffic, as shown in Fig. 4.

3.5 Traffic profile

The traffic profile in Belgium is obtained using on-site measurements of 4G sites. Normalizing the individual traffic profiles of each site by the number of inhabitants in its cell yields similar patterns with amplitudes of the same order of magnitude. The variance in amplitude can be explained by the normalization method which does not consider all the users actually present in the cell, such as tourists or workers. In addition, consumer behavior changes on weekdays and weekends. In Fig. 5,

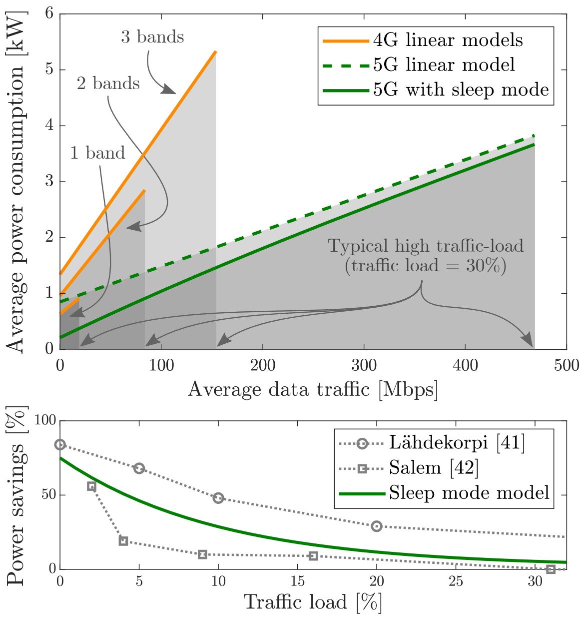

Fig. 4 Power models of all 4G BS types and of 5G BS without and with sleep mode (top), and model of sleep mode power savings compared to two studies (bottom)

the traffic profile is further normalized to have a unit mean over the day and is compared with two normalized profiles from the literature [19, 43]. All these profiles indicate the same trend, with a low traffic during the night and a high traffic during the day. The peak traffic occurs at lunchtime in the profile of this work, whereas it occurs in the afternoon or the evening in the two other profiles. The normalized traffic profile $r(t)$ is independent of the small-scale system configuration and is considered to stay the same over the year.

The small-scale traffic (in Mbps) of a mobile generation xG in a cell of configuration (i, j) is

$$R_{ij}^{xG}(t) = \frac{Pop_{avg,i}^{cell}}{N_{op}} \cdot \alpha_{pop,i}^{xG} \cdot R_{avg,j}^{user,xG} \cdot r(t), \quad (13)$$

where $Pop_{avg,i}^{cell}$ is the average cell population of deployment area i (see Table 1), $\alpha_{pop,i}^{xG}$ is the penetration ratio of xG in deployment area i, and $R_{avg,j}^{user,xG}$ is the daily average throughput per xG user served by a BS of type j. On-site measurements show that the daily average throughput per 4G user is higher when there are more bands installed at the site: +24% for a 2-band BS and +107% for a 3-band BS, compared to a 1-band BS.

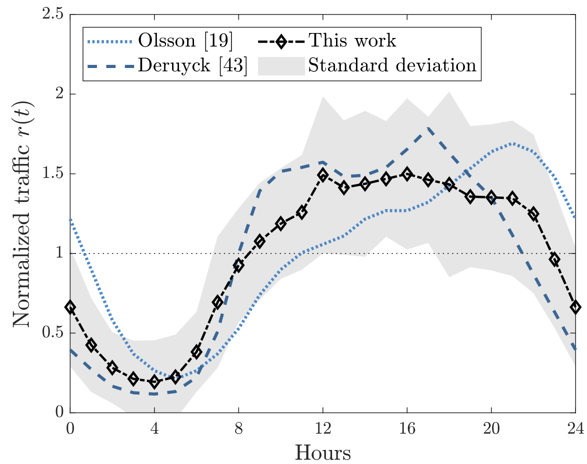

Fig. 5 Normalized traffic profile using measurements compared with two other traffic profiles from the literature

We hypothesize that a larger bandwidth encourages users to consume more data thanks to higher throughput. In addition, sites with a larger bandwidth are installed where high traffic peaks are observed, potentially generated by non-domestic users that are not considered for normalization. M2M traffic is directly included in $R_{avg,j}^{user,xG}$ as the overall traffic generated by humans and machines is normalized per human user only.

4 Scenarios

In 2020, we consider that only 4G is running. We also assume that 4G RANs are fixed for next years, such that no more 4G BS or 4G band will be brought into service by 2025. Regarding 5G, deployment strategies are uncertain, and six scenarios are studied over the 2020-2025 period. When a deployment area is supposed to be covered by 5G, it means that 5G is deployed on all existing 4G sites of this deployment area. It implies that only inhabitants of these cells could use 5G, and that 5G subscriber penetration depends on the scenario. Only one type of 5G BS is considered in this work, and the number of 5G BSs that would be installed in each deployment area is $N_i^{5G} = \sum_{j=1}^{N_{types}^{4G}} N_{ij}^{4G}$. The scenarios are:

(1) **No 5G deployment** (coverage = 0%): only 4G supports the increase in mobile traffic. This scenario is very unlikely as the first phase of 5G deployment has already begun.

Table 5 Parameters of logistic curves that model the number of mobile users and their data traffic

$F(y)$	Unit	K	a	b	Time span	R^2
$\alpha^{5G}_{tot,(s)}(y)$	%	$cov^{5G}_{(s)}$	1.00	2022	$y \geq 2021$	N.A.
$U^{DATA}(y)$	#	$Pop^{\mathrm{BEL}}_{tot}(y)$	0.32	2014	$y \geq 2012$	0.98
$U^{4G}_{(s)}(y) + U^{5G}_{(s)}(y)$	#	$U^{DATA}(y)$	0.53	2015	$y \geq 2012$	0.97
$U^{5G}_{(s)}(y)$	#	$\alpha^{5G}_{tot,(s)}(y) \cdot U^{DATA}(y)$	0.90	2024	$y \geq 2021$	N.A.
$V^{3G}_{user}(y)$	GB	14.00	0.75	2015	$y \geq 2012$	0.87
$V^{4G}_{user,avg}(y)$	GB	84.00	0.53	2020	$y \geq 2015$	0.98
$V^{4G}_{user,1}(y)$	GB	59.64	0.53	2020	$y \geq 2015$	N.A.
$V^{4G}_{user,2}(y)$	GB	73.92	0.53	2020	$y \geq 2015$	N.A.
$V^{4G}_{user,3}(y)$	GB	123.48	0.53	2020	$y \geq 2015$	N.A.
$V^{5G}_{user}(y)$	GB	504.00	0.30	2028	$y \geq 2021$	N.A.

(2) **DU and SDU deployment** (coverage = 37%): only densely populated areas are covered by 5G, increasing the capacity of mobile broadband networks in city centers.
(3) **Urban, DU and SDU deployment** (coverage = 53%): wider 5G coverage is offered by operators in cities, covering more than half of the Belgian population.
(4) **Suburban, urban, DU and SDU deployment** (coverage = 83%): outskirts of cities and villages are also covered by 5G, offering 5G to a major part of the population.
(5) **Full 5G deployment** (coverage = 100%): the entire population is covered by 5G, even isolated homes in the wilderness, such that 4G and 5G coverages are the same.
(6) **Full 5G deployment and 4G decommissioning** (coverage = 100%): the entire population is covered by 5G and 4G BSs are removed. This scenario is unlikely because it requires a stand-alone 5G network by 2025, forcing all 4G users to change their smartphones before.

The total number of mobile data users $U^{DATA}(y)$ is the sum of 3G, 4G and 5G users, respectively $U^{3G}(y)$, $U^{4G}_{(s)}(y)$, and $U^{5G}_{(s)}(y)$, as

$$U^{DATA}(y) = U^{3G}(y) + U^{4G}_{(s)}(y) + U^{5G}_{(s)}(y), \quad (14)$$

where subscript (s) means that variables depend on the scenario. We then suppose that $U^{DATA}(y)$ will saturate at the total population of Belgium $Pop^{\mathrm{BEL}}_{tot}(y)$, which grows linearly by about 56.1 thousand people every year [44]. For each scenario, a different share of mobile users subscribes to 5G between 2020 and 2025, and the others still use 4G or 3G. Hence, the 5G penetration ratio $\alpha^{5G}_{tot,(s)}(y)$ increases over time up to a limit which is the percentage of population covered by 5G $cov^{5G}_{(s)}$. Over one year, an average 4G user transfers a volume of data $V^{4G}_{user,avg}$, and a 5G user transfers a volume of data V^{5G}_{user}. The total volume of mobile data transferred in Belgium during one year is

$$V^{DATA}_{tot,(s)}(y) = V^{3G}_{tot} + U^{4G}_{(s)}(y) \cdot V^{4G}_{user,avg}(y) + U^{5G}_{(s)}(y) \cdot V^{5G}_{user}(y), \quad (15)$$

where the volume of 3G data V^{3G}_{tot} is considered constant over the years, regardless of the scenario.

The modeling and the forecasting of all these variables are based on logistic curves, which allow considering system boundaries, unlike exponential curves [45–47]. Logistic curves are divided into three successive phases: (i) a short-term phase of fast growth (almost exponential), (ii) a mid-term phase of stable increase (almost linear), and (iii) a long-term phase of slower growth and saturation when approaching the upper limit. The basic logistic curve is symmetric between two horizontal asymptotes with an inflection point lying midway between them. Its equation in function of year y is

$$F(y) = \frac{K}{1 + \exp(-a(y - b))}, \quad (16)$$

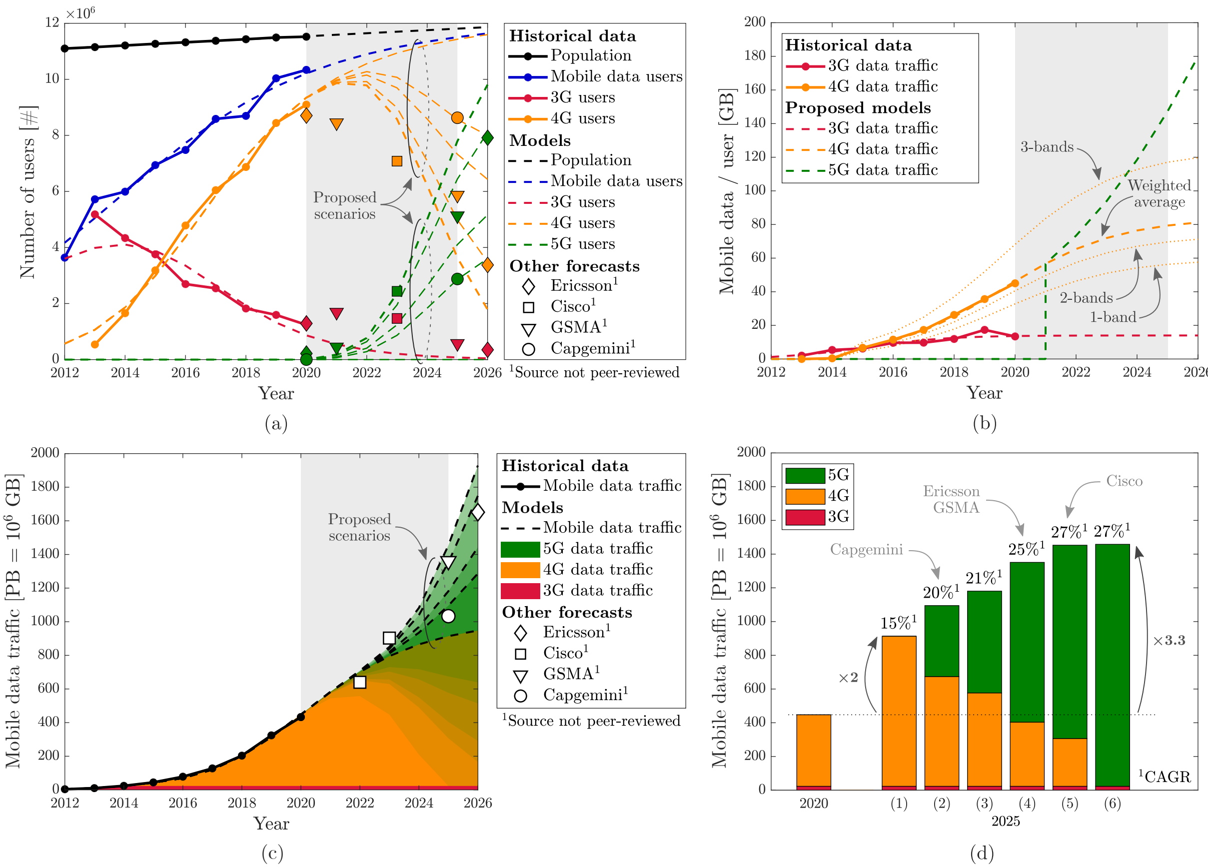

Fig. 6 Historical data, modeling over time and comparison with forecasts from other studies of (a) the number of users per generation compared with the Belgian population, (b) the mobile data traffic per user for each generation, (c) the total mobile data traffic per generation, and (d) a comparison of the reference situation in 2020 with all scenarios in 2025

where K is the saturation level, $a > 0$ indicates the intrinsic growth rate, and b is the time shift in years. Table 5 summarizes the parameters of logistic curves that model the aforementioned variables. Parameters of existing variables are set by curve fitting on historical BIPT data [29], and prospective parameters are set to suit scenarios and to be consistent with Ericsson [12], Cisco [13] and GSMA [14] forecasts for Western Europe, and with Capgemini [48] forecasts for Belgium.

Figure 6(a) shows the number of users per mobile generation between 2012 and 2026. In 2025, a large part of users covered by 5G actually use 5G, and the others still use 3G or 4G despite the availability of 5G. As market penetration is faster for each generation, the intrinsic growth rate of 5G users is greater than for 4G users, itself greater than for mobile data users. The upper bound of traffic per 4G user is set at almost twice as much as in 2020. Therefore, 4G saturation is clearly noticeable in 2025 in Fig. 6(b) [49]. Traffic per 5G user is set to be the same as a 4G user in 2021, but we expect it to grow faster than 4G and reach a much higher upper bound. As a result, only the first exponential phase of the logistic curve is concerned by 2025 with a compound annual growth rate (CAGR) of 25%. The rise of the saturation level between 4G and 5G can be seen as a *rebound mechanism* driven by economic and psychological factors [50, 51]. The same observation can already be made between 3G and 4G. Figure 6(c) shows the total data traffic per mobile generation between 2012 and 2026, and Figure 6(d) compares the reference case in 2020 with the six scenarios in 2025. Without 5G deployment, 4G traffic saturates below 1000 PB which is more than twice the traffic transferred in 2020. When 5G is deployed, the total traffic can increase without saturation in the short term, and it reaches more than 1400 PB in scenarios (5) and (6). In scenario (6), 4G BSs are decommissioned and remaining 4G users are forced to move to 5G. In that case, these users do not change their behavior, and the total data volume in scenarios (5) and (6) remains the same.

5 Results and discussion

This section presents results for each scenario and for two different types of 5G BSs: (i) without SM, and (ii) with SM. The reference year is 2020 and the predicted year is 2025. The two analyzed metrics are the energy consumption of 4G and 5G RANs in Belgium and their respective carbon footprint using a life-cycle approach. These absolute metrics are also normalized by data traffic and by users to obtain energy and carbon intensities.

5.1 Energy consumption

The energy consumption of each mobile generation is the operational electricity of its RAN. In 2020, we estimate that 4G RANs consume 112 GWh, which corresponds to 0.13% of the annual electricity consumption in Belgium (i.e., 84.7 TWh [52]). In 2025, the total energy consumption goes up, especially with extensive 5G deployments, as shown in Fig. 7(a). When 5G is not deployed, the rise in energy consumption is 18% whereas the data traffic doubles. With full 5G deployment, it increases by 81% without SM and only by 27% with SM, while the total data traffic increases more than threefold. This indicates a *relative decoupling* between data traffic and energy consumption [53]. Only scenario (6) with 4G decommissioning shows an *absolute decoupling* over the period of the study, with energy savings of 10% without SM and 63% with SM. This highlights that operating multiple mobile generations in parallel stacks their energy consumptions but does not substitute one for the other. Indeed, the static energy consumption remains unchanged in 4G regardless of the scenario and accounts for 70 to 90% of the total RAN energy. In 5G, the same ratio applies to basic BSs, but it can be greatly improved with SM. Hence, techniques that reduce static power consumption are crucial for low-energy mobile communications.

5.2 Energy intensity

The energy intensity per GB is shown in Fig. 7(c) for 4G and 5G independently, and for both generations together. Clearly, the energy intensity of 5G is 3 to 5× lower compared to 4G, and up to 8 to 12× better with SM. Without 5G deployment, the energy intensity of 4G is 0.15 kWh/GB in 2025, which is 2× lower than in 2020 because the additional traffic requires few more dynamic power, and no more static power. The energy intensity of 5G is minimum in scenario (2), but it increases with more extensive deployments as BSs are less loaded in less populated areas. In scenario (6), energy intensity of 5G is lower than in scenario (5) because 5G BSs are more loaded due to 4G decommissioning. In 2025, the average energy intensity shows an improvement compared to 2020 and is roughly the same for all scenarios with 4G maintained. However, the expected energy savings from this improvement are partly offset by the data traffic increase in scenario (6), and it even *backfires* in all other scenarios as the absolute energy consumption increases between 2020 and 2025. This hence illustrates a *rebound effect* [50, 51, 53]. Therefore, improving the energy efficiency of a mobile communication technology does not directly reduce its total energy consumption.

By dividing the energy consumption of broadband RANs by their respective number of mobile users, the energy intensity is still better in 5G than in 4G, and 5G is once again enhanced with SM, as shown in Fig. 7(e). But, unlike the data traffic, the total number of mobile broadband users grows slower than the energy consumption, and no reduction in average energy intensity per user occurs between 2020 and 2025 when 4G is maintained. It even increases when 5G is deployed without SM, and only 4G decommissioning can reduce the average energy per user in 2025. We estimate that the energy intensity remains around 12 kWh/user in 2025 when using SM in 4G and maintaining 4G. In order not to increase the RAN energy consumption while offering mobile Internet access to the same number of users, MNOs should not operate 5G without SM in parallel with 4G.

5.3 Carbon footprint

The carbon footprint of RANs consists of embodied and operating GHG emissions. The operating carbon footprint is estimated using the carbon

The version of the Article published by the journal is available at: http://dx.doi.org/10.1007/s12243-022-00932-9.

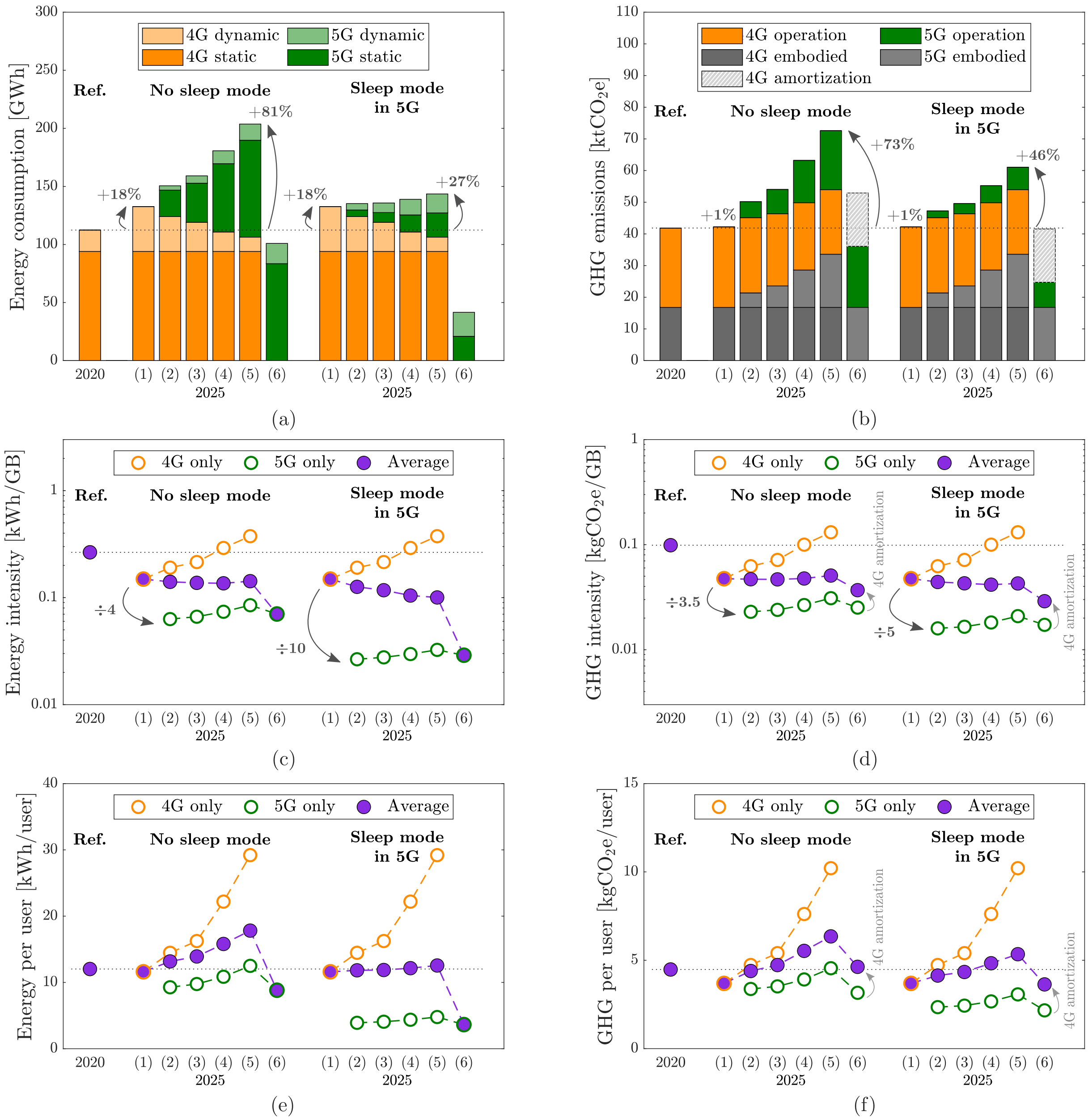

Fig. 7 Results in the reference situation in 2020 and for each scenario in 2025 without and with sleep mode for (a) total electricity consumption, (b) total GHG emissions, (c) energy intensity per GB, (d) carbon intensity per GB, (e) energy intensity per user, and (f) carbon intensity per user

intensity of electricity consumed in Belgium, i.e., 0.230 $kgCO_2e/kWh$ in 2019 [54]. Assuming a reduction rate of 3% per year as observed in historical trends [52], the power carbon intensity is projected to be 0.223 $kgCO_2e/kWh$ in 2020, and 0.192 $kgCO_2e/kWh$ in 2025. The embodied carbon footprint is more uncertain as very few studies assess it, in addition to poorly describing their scope. For one BS of any mobile generation, it ranges from 12 to 35 tCO_2e with a lifetime of 10 to 20 years [55–58]. In this work, we assume an embodied carbon footprint of 18 tCO_2e per 4G and 5G BS with a lifetime of 12 years, giving 1.5 tCO_2e/BS/year. In 2020, we evaluate a total carbon footprint of 42 $ktCO_2e$ for 4G RANs. Without 5G deployment in 2025, Fig. 7(b) shows

The version of the Article published by the journal is available at: http://dx.doi.org/10.1007/s12243-022-00932-9.

that the increase in 4G energy consumption is balanced by the decrease of power carbon intensity, such that the total carbon footprint remains the same. When rolling out 5G, new BSs need to be produced to cover new areas. In scenario (5), the embodied carbon footprint is equivalent in 4G and 5G as there are the same number of BSs for each generation. In this case, total emissions increase by 73% compared to 2020, and by 46% with SM. In scenario (6), embodied emissions of 4G BSs are represented as carbon amortization because its 12-year embodied carbon footprint must be still counted even if 4G is no longer active, to fairly compare with other scenarios. All together, embodied emissions account for 40% of the total 4G carbon footprint in 2020, and up to 45% in 2025. For 5G, it accounts for 48% without SM, and up to 70% with SM. Even if these emissions are quite uncertain, they are non-negligible and should be taken into account in mobile network deployment strategies. Including amortization of 4G BSs, none of the scenarios significantly reduce total GHG emissions of broadband RANs in 2025.

5.4 Carbon intensity

As for energy consumption, the total carbon footprint per generation is divided by the volume of mobile data and by the number of users to provide carbon intensities. The same trends as for energy intensities are observed in Fig. 7(d) and Fig. 7(f), with lower carbon intensities for 5G than for 4G. However, the reduction of 5G carbon intensities thanks to SM is less important than for energy because embodied emissions do not change with this feature. The average carbon intensity of mobile data transfers is estimated to be 0.10 $kgCO_2$/GB in 2020 and around 0.05 $kgCO_2$/GB in 2025 for scenarios keeping 4G active, even with SM in 5G. Again, a *rebound effect* appears for the carbon footprint. Per user, the average carbon intensity remains between 4 and 6 $kgCO_2e$/user for all scenarios. The amortization of 4G BSs reduces GHG emission savings.

6 Conclusion

In this work, we present a method to evaluate and to project the total energy consumption of country-wide broadband RANs. We use on-site measurements to derive power models of 4G BSs, which show a linear relationship between power consumption and data traffic with a static power component. We then build a prospective power model of 5G BSs by scaling 4G models with respect to bandwidth, number of data streams, and expected technological improvements.

Results show that the RAN energy consumption is mostly independent of the data traffic because BSs are lightly loaded on average. Without 5G deployment, we predict that the annual mobile data traffic in Belgium saturates in 2025 at twice the data volume of 2020, whereas the total energy consumption of 4G RANs increases by 18% only. With full 5G deployment, we rather predict a threefold growth in mobile data traffic and an 81% increase in total energy consumption, despite the improvement in energy intensity. This illustrates a *backfire rebound effect*. The sleep mode feature can reduce the static energy consumption of 5G, improving up to 10 times its energy efficiency compared to 4G. If 4G is additionally decommissioned, the total RAN energy consumption can drop, but this scenario is very unlikely by 2025. Therefore, we show that concurrently operating country-wide 4G and 5G RANs consumes more energy than using only one generation. This finding calls for sufficiency policies in future deployments of mobile communication networks.

Accurately assessing environmental impacts of 4G and 5G BSs throughout their life-cycle is difficult because there is currently a lack of data and information from manufacturers. Hence, we roughly estimate embodied and operating GHG emissions of BSs, and we observe a clear upward trend of RAN carbon footprint when 5G deployment is extensive. This is partly due to the large number of new 5G BSs that need to be produced. Depending on the scenario, embodied GHG emissions account for 40 to 70% of the total carbon footprint, which is significant and should be included in mobile network deployment strategies.

Future work is needed to validate power models of 5G BSs with on-site measurements. In addition, BS power models should be refined for time intervals shorter than one hour, in order to capture faster traffic fluctuations. The deployment of enhanced mobile communication networks also affects other segments of ICTs, such that prospective evaluation studies should also include end-user devices, data centers and core networks.

The version of the Article published by the journal is available at: http://dx.doi.org/10.1007/s12243-022-00932-9.

Declarations

Funding. This study was partly funded by Proximus NV/SA.

Conflict of interest. The authors declare they have no competing interests.

References

[1] Malmodin, J., Lundén, D.: The energy and carbon footprint of the global ICT and E&M sectors 2010–2015. Sustainability **10**(9), 3027 (2018). https://doi.org/10.3390/su10093027

[2] Andrae, A.: New perspectives on Internet electricity use in 2030. Engineering and Applied Science Letters **3**, 19–31 (2020). https://doi.org/10.30538/psrp-easl2020.0038

[3] Belkhir, L., Elmeligi, A.: Assessing ICT global emissions footprint: Trends to 2040 & recommendations. Journal of Cleaner Production **177**, 448–463 (2018). https://doi.org/10.1016/j.jclepro.2017.12.239

[4] Freitag, C., Berners-Lee, M., Widdicks, K., Knowles, B., Blair, G., Friday, A.: The real climate and transformative impact of ICT: A critique of estimates, trends, and regulations. Patterns **2**, 100340 (2021). https://doi.org/10.1016/j.patter.2021.100340

[5] Bordage, F.: The environmental footprint of the digital world. GreenIT.fr (2019)

[6] GeSI, BCG: SMARTer 2020 - The role of ICT in driving a sustainable future (2012)

[7] GeSI, Accenture: #SMARTer2030 - ICT solutions for 21st century challenges (2015)

[8] Bol, D., Pirson, T., Dekimpe, R.: Moore's law and ICT innovation in the Anthropocene. In: 2021 Design, Automation & Test in Europe Conference & Exhibition (DATE), pp. 19–24 (2021). https://doi.org/10.23919/DATE51398.2021.9474110

[9] IPCC: Summary for policymakers. In: Climate Change 2022, Mitigation of Climate Change, AR6, WGIII. Cambridge University Press (2022). https://doi.org/10.1017/9781009157926.001

[10] Fehske, A., Malmodin, J., Biczók, G., Fettweis, G.: The global carbon footprint of mobile communications - The ecological and economic perspective. IEEE Communications Magazine **49** (2011). https://doi.org/10.1109/MCOM.2011.5978416

[11] Pihkola, H., Hongisto, M., Apilo, O., Lasanen, M.: Evaluating the energy consumption of mobile data transfer — From technology development to consumer behaviour and life cycle thinking. Sustainability **10**(7), 2494 (2018). https://doi.org/10.3390/su10072494

[12] Ericsson, AT&T: Mobility report (2020)

[13] Cisco: Annual Internet report (2018–2023) (2020)

[14] GSMA: The mobile economy 2021 (2021)

[15] Al-Falahy, N., Alani, O.Y.: Technologies for 5G networks: Challenges and opportunities. IT Professional **19**(1), 12–20 (2017). https://doi.org/10.1109/MITP.2017.9

[16] Malmodin, J.: The power consumption of mobile and fixed network data services - The case of streaming video and downloading large files. In: Proceedings of Electronics Goes Green 2020+ (2020)

[17] Santarius, T., Bieser, J.C.T., Frick, V., Höjer, M., Gossen, M., Hilty, L.M., Kern, E., Pohl, J., Rohde, F., Lange, S.: Digital sufficiency: conceptual considerations for ICTs on a fnite planet. Annals of Telecommunications (2022). https://doi.org/10.1007/s12243-022-00914-x

[18] Auer, G., Giannini, V., Desset, C., Godor, I., Skillermark, P., Olsson, M., Imran, M.A., Sabella, D., Gonzalez, M.J., Blume, O., Fehske, A.: How much energy is needed to run a wireless network? IEEE Wireless Communications **18**(5), 40–49 (2011). https://doi.org/10.1109/MWC.2011.6056691

The version of the Article published by the journal is available at: http://dx.doi.org/10.1007/s12243-022-00932-9.

[19] Olsson, M., Tombaz, S., Gódor, I., Frenger, P.: Energy performance evaluation revisited: Methodology, models and results. In: 2016 IEEE 12th International Conference on Wireless and Mobile Computing, Networking and Communications (WiMob), pp. 1–7 (2016). https://doi.org/10.1109/WiMOB.2016.7763182

[20] Lorincz, J., Garma, T.: Measurements and modelling of base station power consumption under real traffic loads. Sensors (Basel, Switzerland) **12**, 4181–310 (2012). https://doi.org/10.3390/s120404281

[21] Deruyck, M., Joseph, W., Martens, L.: Power consumption model for macrocell and microcell base stations. Transactions on Emerging Telecommunications Technologies **25**(3), 320–333 (2014). https://doi.org/10.1002/ett.2565

[22] Dahal, M., Shrestha, J., Shakya, S.: Comparison & measurement of energy efficiency of micro and macro base stations in Nepal using regression model. Journal of Green Engineering **7**, 505–526 (2018). https://doi.org/10.13052/jge1904-4720.743

[23] Lorincz, J., Matijevic, T., Petrovic, G.: On interdependence among transmit and consumed power of macro base station technologies. Computer Communications **50**, 10–28 (2014). https://doi.org/10.1016/j.comcom.2014.02.010

[24] Grøndalen, O., Zanella, A., Mahmood, K., Carpin, M., Rasool, J., Østerbø, O.N.: Scheduling policies in time and frequency domains for LTE downlink channel: A performance comparison. IEEE Transactions on Vehicular Technology **66**(4), 3345–3360 (2017). https://doi.org/10.1109/TVT.2016.2589462

[25] BIPT: Atlas Mobile. https://www.bipt-data.be/fr/projects/atlas/mobile Accessed 2021-02-14

[26] Geoportail de Wallonie: Cadastre des Antennes émettrices Stationnaires de Wallonie. https://geoportail.wallonie.be/walonmap#SHARE=C300838ACD2B2802E053D0AFA49D9390 Accessed 2021-03-05

[27] Bruxelles Environnement: Carte des Antennes émettrices à Bruxelles. https://geodata.environnement.brussels/client/view/3a33e35f-6b64-4b28-bb50-5b4c6b7cb29c Accessed 2021-03-09

[28] Geopunt Vlaanderen: Zendantennes. http://www.geopunt.be/catalogus/datasetfolder/00b8c6b6-437d-4d35-9b39-7ad300f11b94 Accessed 2021-03-11

[29] BIPT: Rapport annuel 2020 (2021)

[30] IWEPS: Degré de Densité de la Population des Communes Belges. https://www.iweps.be/indicateur-statistique/degre-de-densite-de-population-communes-belges-metho Accessed 2021-03-19

[31] Parkvall, S., Furuskär, A., Dahlman, E.: Evolution of LTE toward IMT-Advanced. IEEE Communications Magazine **49**(2), 84–91 (2011). https://doi.org/10.1109/MCOM.2011.5706315

[32] Debaillie, B., Desset, C., Louagie, F.: A flexible and future-proof power model for cellular base stations. In: 2015 IEEE 81st Vehicular Technology Conference (VTC Spring), pp. 1–7 (2015). https://doi.org/10.1109/VTCSpring.2015.7145603

[33] Fuentes, M., Carcel, J., Dietrich, C., Yu, L., Garro, E., Volker, P., Lazarakis, F., Grondalen, O., Bulakci, O., Yu, J., Mohr, W., Gomez-Barquero, D.: 5G new radio evaluation against IMT-2020 key performance indicators. IEEE Access **8**, 110896 (2020). https://doi.org/10.1109/ACCESS.2020.3001641

[34] Lei, W., Soong, A., Jianghua, L., Yong, W., Classon, B., Xiao, W., Mazzarese, D., Yang, Z., Saboorian, T.: 5G System Design: An End to End Perspective. Springer, Switzerland (2021). https://doi.org/10.1007/978-3-030-73703-0

[35] Halvarsson, B., Simonsson, A., Elgcrona, A., Chana, R., Machado, P., Asplund, H.: 5G NR testbed 3.5 GHz coverage results. In: 2018 IEEE 87th Vehicular Technology Conference (VTC Spring), pp. 1–5 (2018). https://doi.org/10.1109/VTCSpring.2018.8417704

[36] Sun, L., Ding, Z., Guo, D., Yan, L., Yan, C.: High efficiency high density telecom rectifier with GaN device. In: 2015 IEEE International Telecommunications Energy Conference (INTELEC), pp. 1–5 (2015). https://doi.org/10.1109/INTLEC.2015.7572401

[37] Oh, S.-J.: IMT-2020 Evaluation report. TTA SPG33 (2019)

[38] 3GPP: TDocs at Gothenburg Meeting. https://www.3gpp.org/DynaReport/TDocExMtg--R1-94--18796.htm Accessed 2021-05-29

[39] Usama, M., Erol-Kantarci, M.: A survey on recent trends and open issues in energy efficiency of 5G. Sensors **19**(14), 3126 (2019). https://doi.org/10.3390/s19143126

[40] Frenger, P., Tano, R.: More capacity and less power: How 5G NR can reduce network energy consumption. In: 2019 IEEE 89th Vehicular Technology Conference (VTC2019-Spring), pp. 1–5 (2019). https://doi.org/10.1109/VTCSpring.2019.8746600

[41] Lähdekorpi, P., Hronec, M., Jolma, P., Moilanen, J.: Energy efficiency of 5G mobile networks with base station sleep modes. In: 2017 IEEE Conference on Standards for Communications and Networking (CSCN), pp. 163–168 (2017). https://doi.org/10.1109/CSCN.2017.8088616

[42] Salem, F.E., Chahed, T., Altman, Z., Gati, A.: Traffic-aware advanced sleep modes management in 5G networks. In: 2019 IEEE Wireless Communications and Networking Conference (WCNC), pp. 1–6 (2019). https://doi.org/10.1109/WCNC.2019.8886051

[43] Deruyck, M., Joseph, W., Tanghe, E., Martens, L.: Reducing the power consumption in LTE-Advanced wireless access networks by a capacity based deployment tool. Radio Science **49** (2014). https://doi.org/10.1002/2013RS005364

[44] StatBel: Structure de la Population. https://statbel.fgov.be/fr/themes/population/structure-de-la-population#figures Accessed 2021-04-11

[45] Kucharavy, D., De Guio, R.: Logistic substitution model and technological forecasting. Procedia Engineering **9** (2011). https://doi.org/10.1016/j.proeng.2011.03.129

[46] Jha, A., Saha, D.: Forecasting and analysing the characteristics of 3G and 4G mobile broadband diffusion in India: A comparative evaluation of Bass, Norton-Bass, Gompertz, and logistic growth models. Technological Forecasting and Social Change **152**, 119885 (2020). https://doi.org/10.1016/j.techfore.2019.119885

[47] Shin, H., Jung, J., Koo, Y.: Forecasting the video data traffic of 5G services in South Korea. Technological Forecasting and Social Change **153**, 119948 (2020). https://doi.org/10.1016/j.techfore.2020.119948

[48] BIPT, Capgemini: Evolution des données mobiles liées au spectre sous licence en Belgique et impact sur la présence des médias (2020)

[49] BIPT: Risques de saturation des réseaux mobiles (2021)

[50] Lange, S., Kern, F., Peuckert, J., Santarius, T.: The Jevons paradox unravelled: A multi-level typology of rebound effects and mechanisms. Energy Research & Social Science **74**, 101982 (2021). https://doi.org/10.1016/j.erss.2021.101982

[51] Reimers, H., Jacksohn, A., Appenfeller, D., Lasarov, W., Hüttel, A., Rehdanz, K., Balderjahn, I., Hoffmann, S.: Indirect rebound effects on the consumer level: A state-of-the-art literature review. Cleaner and Responsible Consumption **3**, 100032

(2021). https://doi.org/10.1016/j.clrc.2021.100032

[52] IEA: Data and Statistics for Belgium. https://www.iea.org/data-and-statistics/data-browser?country=BELGIUM Accessed 2021-06-03

[53] Hilty, L.M., Aebischer, B.: ICT Innovations for Sustainability. Springer, Switzerland (2015). https://doi.org/10.1007/978-3-319-09228-7

[54] Scarlat, N., Prussi, M., Padella, M.: Quantification of the carbon intensity of electricity produced and used in Europe. Applied Energy **305**, 117901 (2022). https://doi.org/10.1016/j.apenergy.2021.117901

[55] Malmodin, J., Lundén, D., Moberg, A., Andersson, G., Nilsson, M.: Life cycle assessment of ICT. Journal of Industrial Ecology **18**(6), 829–845 (2014). https://doi.org/10.1111/jiec.12145

[56] Humar, I., Ge, X., Xiang, L., Jo, M., Chen, M., Zhang, J.: Rethinking energy efficiency models of cellular networks with embodied energy. IEEE Network **25**(2), 40–49 (2011). https://doi.org/10.1109/MNET.2011.5730527

[57] Bergmark, P.: Life cycle assessment of an LTE base station based on primary data. Third ETSI Workshop on ICT Energy Efficiency and Environmental Sustainability (2015)

[58] Bieser, J., Salieri, B., Hischier, R., Hilty, L.: Next generation mobile networks: Problem or opportunity for climate protection? (2020)